Clim Dyn (2014) 43:2747–2763
DOI 10.1007/s00382-014-2091-y

The eastward shift of the Walker Circulation in response to global warming and its relationship to ENSO variability

Tobias Bayr · Dietmar Dommenget · Thomas Martin · Scott B. Power

Received: 28 October 2013 / Accepted: 11 February 2014 / Published online: 11 March 2014

Abstract This study investigates the global warming response of the Walker Circulation and the other zonal circulation cells (represented by the zonal stream function), in CMIP3 and CMIP5 climate models. The changes in the mean state are presented as well as the changes in the modes of variability. The mean zonal circulation weakens in the multi model ensembles nearly everywhere along the equator under both the RCP4.5 and SRES A1B scenarios. Over the Pacific the Walker Circulation also shows a significant eastward shift. These changes in the mean circulation are very similar to the leading mode of interannual variability in the tropical zonal circulation cells, which is dominated by El Niño Southern Oscillation variability. During an El Niño event the circulation weakens and the rising branch over the Maritime Continent shifts to the east in comparison to neutral conditions (vice versa for a La Niña event). Two-thirds of the global warming forced trend of the Walker Circulation can be explained by a long-term trend in this interannual variability pattern, i.e. a shift towards more El Niño-like conditions in the multi-model mean under global warming. Further, interannual variability in the zonal circulation exhibits an asymmetry between El Niño and La Niña events. El Niño anomalies are located more to the east compared with La Niña anomalies. Consistent with this asymmetry we find a shift to the east of the dominant mode of variability of zonal stream function under global warming. All these results vary among the individual models, but the multi model ensembles of CMIP3 and CMIP5 show in nearly all aspects very similar results, which underline the robustness of these results. The observed data (ERA Interim reanalysis) from 1979 to 2012 shows a westward shift and strengthening of the Walker Circulation. This is opposite to what the results in the CMIP models reveal. However, 75 % of the trend of the Walker Circulation can again be explained by a shift of the dominant mode of variability, but here towards more La Niña-like conditions. Thus in both climate change projections and observations the long-term trends of the Walker Circulation seem to follow to a large part the pre-existing dominant mode of internal variability.

Keywords Global warming · Walker Circulation · Zonal atmospheric circutlation · ENSO variability · Asymmetry of ENSO · Changes in the modes of variability

1 Introduction

The equatorial zonal circulation of the atmosphere originates from the zonal temperature differences along the equator mainly due to the land-sea distribution and ocean circulation within the tropics. The main zonal circulation cells are the Indian Ocean cell, the Pacific Ocean cell (or Walker Circulation) and the Atlantic Ocean cells (Hastenrath 1985). The Walker Circulation is the most prominent and its variability is strongly linked to sea surface temperature (SST) variations associated with the El Niño Southern Oscillation (ENSO) phenomenon (Philander

T. Bayr (✉) · T. Martin
GEOMAR Helmholtz Centre for Ocean Research, Düsternbrooker Weg 20, 24105 Kiel, Germany
e-mail: tbayr@geomar.de

D. Dommenget
School of Mathematical Sciences, Monash University, Clayton, VIC, Australia

S. B. Power
Bureau of Meteorology, CAWCR, GPO Box 1289, Melbourne, VIC 3001, Australia

1990). Mean state and variability of these zonal circulation cells have large socio-economical impacts via modulating the distribution of e.g. precipitation, severe weather and stream flow (e.g. Power et al. 1999). It is therefore of great interest to know how the zonal circulation cells might change—both in mean state and in terms of the variability they exhibit—in response to a warmer climate, and whether they have already changed.

Most recent studies focus on the Walker Circulation and predict that it weakens under global warming (Knutson and Manabe 1995; Vecchi and Soden 2007; DiNezio et al. 2009; Power and Kociuba 2011). This picture has not changed in the climate model runs of the 5th Phase of the Coupled Model Intercomparison Project (CMIP), that were carried out for the 5th Assessment Report (AR5) of the Intergovernmental Panel on Climate Change (IPCC): Figure 1 shows the trend of the strength of the Walker Circulation based on the sea level pressure (SLP) and SST gradient over the equatorial Pacific of the individual CMIP3 models under the A1B scenario and of the individual CMIP5 models under the RCP4.5 scenario. The multi-model mean (MMM) and most individual models show a consistent reduction in both SST and SLP gradients, i.e. a weakening of the Walker Circulation. The CMIP5 ensemble weakens more than the CMIP3 ensemble. This occurs despite a more modest greenhouse gas increase in the CMIP5 RCP4.5 scenario than in the CMIP3 A1B scenario used here. Note, however, that in both the CMIP3 and CMIP5 ensembles are individual models that show no significant trend, and in some cases even a strengthening of the Walker Circulation.

Knutson and Manabe (1995) indicate two different mechanisms which determine the global warming response of the Walker Circulation and the tropical circulations more generally. The first mechanism works with spatially homogeneous warming in the free atmosphere that increases with height. In this situation the hydrological cycle is strengthened, and this leads to enhanced upper level warming, thereby increasing the static stability. This first mechanism was further investigated by Held and Soden (2006) and Vecchi and Soden (2007), who concluded that atmospheric warming weakens the tropical circulations. In contrast an atmospheric cooling strengthens the tropical circulation, as found in a paleo-climate study (DiNezio et al. 2011). In the following we will refer to this mechanism as the homogeneous warming mechanism, as it does not require any horizontal gradients in the warming pattern.

The second mechanism requires spatially inhomogeneous temperature changes, i.e. changes in zonal temperature gradients. This depends on regional differences in the strength of evaporative cooling (Knutson and Manabe 1995), the ocean dynamical thermostat cooling (Clement et al. 1996), cloud cover feedbacks (Meehl and Washington 1996) and the land-sea warming contrast (Bayr and Dommenget 2013a), thus mostly on the interaction between the surface and the atmosphere. For the Walker Circulation, DiNezio et al. (2009) found that in the CMIP3 ensemble the evaporative cooling and cloud cover feedbacks reduce the warming over the warm pool region more effectively than the ocean dynamical thermostat cools the cold tongue region. This reduces the SST gradient over the Pacific and weakens the Walker Circulation. In general, this second mechanism can act in both directions in a warmer climate: it can weaken or strengthen the zonal temperature gradients, thus the zonal circulation. In the following we will refer to this mechanism as the inhomogeneous warming mechanism, as it requires changes in the zonal temperature gradients.

The focus in most recent studies has been on the strength of the Walker Circulation, thus if it is weakening under global warming. However, an upward shift of the Walker Circulation under global warming has also been noted in Haarsma and Selten (2012). The physical mechanisms responsible for the upward shift were investigated by Singh and O'Gorman (2012). They found that increasing tropospheric warming causes both weakening and an upward shift of the general circulation, consistent with the first mechanism above. Further, Vecchi and Soden (2007) and Yu et al. (2012) found in addition to the weakening of the Walker Circulation an eastward shift under global warming. Both studies indicate, that the eastward shift is related to a trend towards more El Niño-like conditions.

ENSO is a coupled air-sea interaction phenomena with associated changes in SST gradient, SLP gradient and surface winds over the Pacific (Philander 1990): El Niño is characterised by anomalous warm SST over the East and Central Pacific, weaker surface winds over the West Pacific, a weaker SLP gradient over the Pacific and more convection over the Eastern Pacific. For La Niña the situation is vice versa, with more convection over the West Pacific, thus ENSO variability is associated with a zonal shift of convection. Another important feature of ENSO variability is its spatial asymmetry (e.g. Hoerling et al. 1997; Rodgers et al. 2004; Yu and Kim 2011; Dommenget et al. 2013), i.e. that the warming of SST during El Niño events occurs further to the east than the SST cooling during La Niña events.

The aim of this study is to investigate the eastward shift of the Walker Circulation under global warming and its relationship to ENSO variability. Further, we want to analyse the changes in the modes of variability and find out if the trends of the zonal circulation cells follow a pre-existing mode of internal variability. In our analyses we use the zonal stream function for the representation of the zonal circulation cells, including the Walker Circulation, as

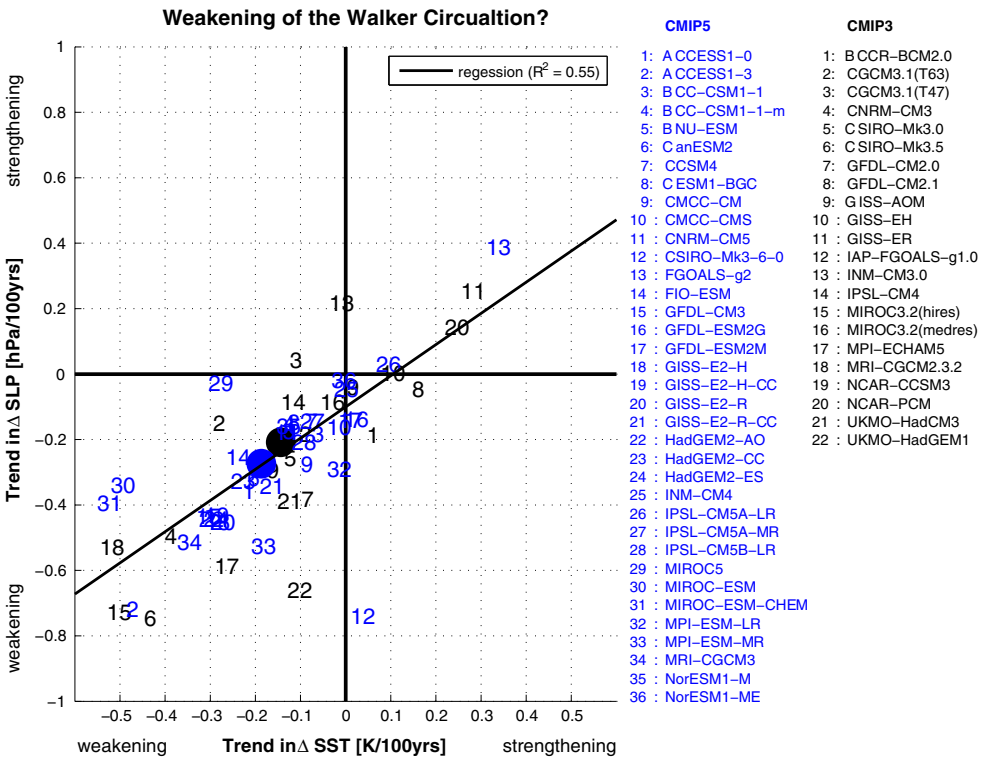

Fig. 1 Trend of the Δbox index difference (W − E) of SST and (E − W) of SLP in the individual models of the CMIP3 and CMIP5 data base, with box E = (80°W–160°W, 5°S–5°N) and box W = (80°E–160°E, 5°S–5°N) over the period 1950–2099; The *black and blue circles* are the multi model mean (MMM) values

defined by Yu and Zwiers (2010) and Yu et al. (2012). This is a direct measure of the circulation in the free atmosphere, in contrast to surface based SLP indices (e.g. Vecchi et al. 2006; Power and Kociuba 2011). The use of the stream function has the advantage that it splits up the convective flow in the zonal and the meridional part and measures the zonal circulation over all levels (Schwendike et al. 2014). Thus it includes both areas where the two mechanisms mentioned above influence the zonal circulation.

We address the following questions: (1) What is the response of the zonal circulation cells to global warming in the mean state and how does this change project onto variability linked to ENSO? (2) Does the Walker Circulation shift eastward and if yes, what causes the eastward shift under global warming? (3) Do the modes of variability of zonal stream function change? (4) Is the projected response already evident in reanalysis data for recent decades? The paper is organised as follows: Sect. 2 gives an overview of the data and the definition of the zonal stream function used in this study. The response of the mean state in the CMIP multi model ensembles is shown in Sect. 3. The eastward shift is examined in Sect. 4. The asymmetry of the Walker Circulation in ENSO variability is investigated in Sect. 5 and the changes in the modes of variability in Sect. 6. The trends in recent decades evident in reanalysis data are discussed in Sect. 7. In Sect. 8 we discuss how changes in SLP relate to changes in the zonal circulation cells. A summary and discussion are provided in Sect. 9.

2 Data and methods

The data analysed in this study are taken from the Climate Model Intercomparison Project Phases 3 and 5 (CMIP3, Meehl et al. 2007 and CMIP5, Taylor et al. 2012). From CMIP3 we use data from the 20C simulation and for the 21C under the A1B scenario. From CMIP5 we use the historical simulations and 21C simulations under the RCP4.5 scenario. The RCP4.5 scenario has an overall smaller increase in greenhouse gases than the A1B scenario and only a weak increase in greenhouse gases from 2050 onward. We choose these greenhouse gas emission scenarios because most of the available models simulated these scenarios; see legend in Fig. 1 for a list of climate models. The following variables from 22 CMIP3 models and 36 CMIP5 models are examined: sea level pressure (SLP), sea surface temperature (SST), atmospheric temperature (T), tropospheric temperature (T_{tropos}; mass weighted average of atmospheric temperature between 1,000 and 100 hPa), zonal wind (U), meridional wind (V) and vertical wind (W). Each data set is interpolated onto a regular 2.5° × 2.5° grid. Separate ensembles are developed for CMIP3 and CMIP5 using one ensemble member for each model. For the trend analysis in Sect. 3 we calculate the multi-model mean (MMM). For all other analysis we concatenate the data sets of the individual models to get one long data set for the multi model ensemble (MME), where detrended anomalies are defined for each model individually first.

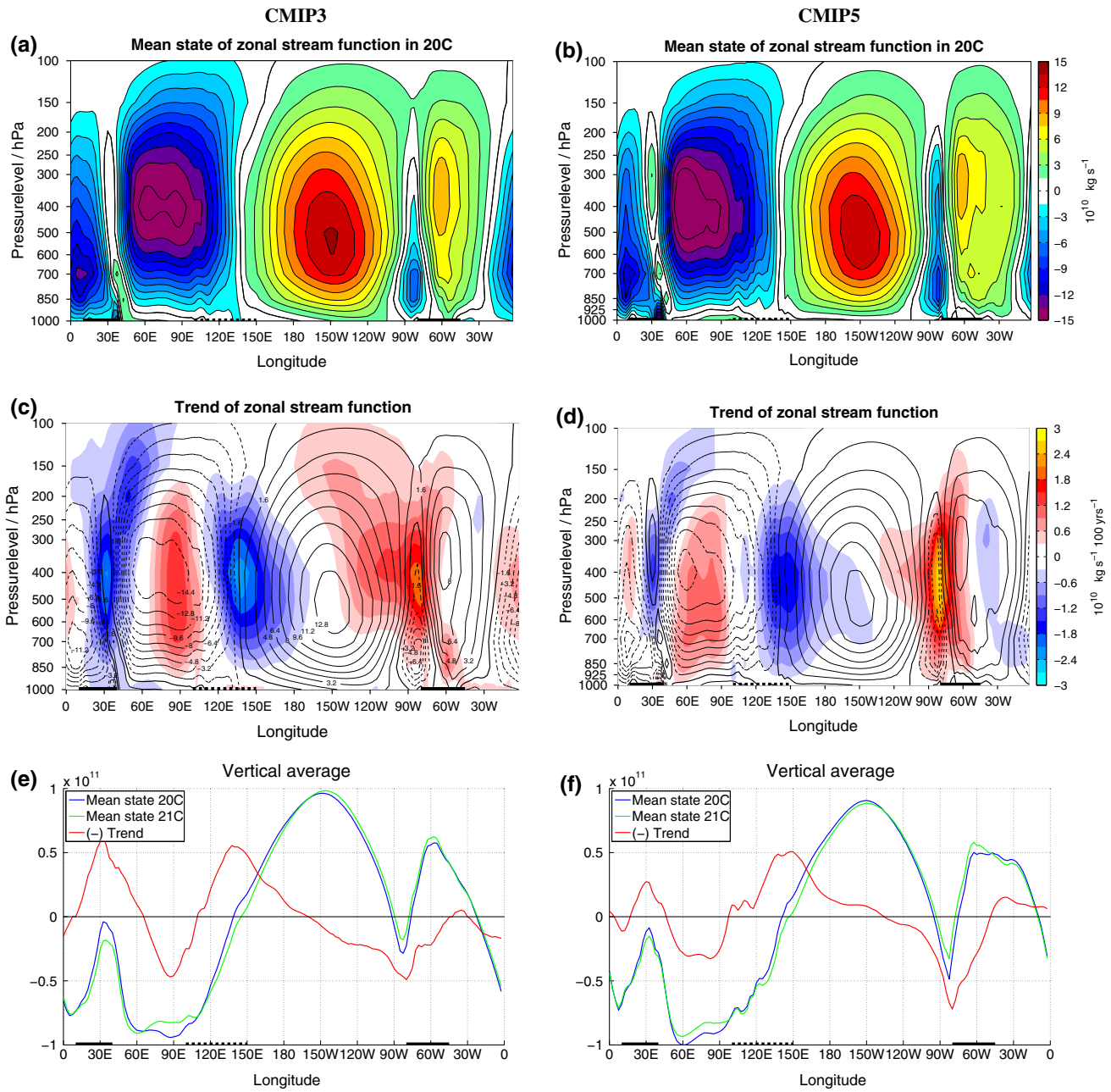

Fig. 2 **a** Mean state of zonal stream function along the equator in CMIP3 MMM over the period from 1950 to 1979 (20C), averaged from 5°S to 5°N; *black bold lines* at the *bottom* indicate the three continents Africa, Maritime Continent and South America, **b** same as **a** but here for CMIP5 MMM, **c** *shading* linear trend of zonal stream function in CMIP3 MMM in the period from 1950 to 2099, contours: mean state from **a**, **d** same as **c** but here for CMIP5 MMM, **e** vertical average of **a** in kg s^{-1} *blue line*, **c** in kg s^{-1} (500 year)$^{-1}$ (*red line*) and mean state over the period from 2070 to 2099 in kg s^{-1} (21C) (*green line*), **f** vertical average of **b** in kg s^{-1} (*blue line*) and **d** in kg s^{-1} (500 year)$^{-1}$ (*red line*) and mean state in 21C in kg s^{-1} (*green line*)

For comparison with observations and analysing the trends over recent decades we use ERA Interim reanalysis data (Simmons et al. 2007) for the period from 1979 to 2012. We choose ERA Interim because the tropical tropospheric temperature trends in this data set are in a good agreement with satellite observations (Bengtsson and Hodges 2009). These data sets are also interpolated onto a regular 2.5° × 2.5° grid.

As a measure for the zonal circulation along the equator we use the zonal stream function as defined in Yu and Zwiers (2010) and Yu et al. (2012):

$$\Psi = 2\pi a \int_0^p u_D \frac{dp}{g}$$

with the divergent component of the zonal wind u_D, the radius of the earth a, the pressure p and gravity constant g. The zonal wind is averaged for the meridional band between 5°N and 5°S and integrated from the top of the atmosphere to surface. In the figures only the levels below 100 hPa are shown, as the stream function is nearly zero above that level.

3 Mean state and response

The mean state of the zonal stream function in the CMIP3 and CMIP5 multi-model mean (MMM) for the period 1950 until 1979 agree quite well with each other (see Fig. 2a, b) and with reanalysis data (not shown), as already investigated previously for CMIP3 (Yu et al. 2012). Positive values indicate a clockwise circulation and negative values an anticlockwise circulation. The three main convection regions (Africa, the Maritime Continent and South America) and the descending regions (West Indian Ocean, the Pacific cold tongue region and the Atlantic Ocean) together form the main circulation cells (the Indian Ocean cell, the Pacific Ocean cell and the Atlantic Ocean cells). The trend patterns under global warming over the period 1950 until 2099 are very similar in the CMIP3 and CMIP5 (Fig. 2c, d) and to the results of Yu et al. (2012). Thus, the trend pattern seems to be very robust despite different models, resolutions, ensemble sizes and emission scenarios in the different ensembles. The MMMs project more ascending over the West Indian Ocean and the Pacific and more descending over Africa, the Maritime Continent and South America under global warming (see also Fig. 3).

We can build the mass weighted vertical averages of the stream functions to get a clearer picture: The global warming trend of the tropical zonal circulations over most of the Indian and Atlantic Ocean is opposite to the mean state (Fig. 2e, f, note the reversed sign of the trend for better comparison), which indicates a weakening of the circulation in agreement with the arguments of Vecchi and Soden (2007). If we focus on the Pacific Ocean, the MMM change in the strength of the circulation (the maximum of the Pacific cell at 150°W) is weak: in the CMIP3 MMM it slightly increases, in agreement with the results of Yu et al. (2012). In the CMIP5 MMM the strength of the circulation slightly decreases. The striking difference between the mean states in the period from 1950 to 1979 (20C) and the period from 2070 to 2099 (21C) over the Pacific evident is the eastward shift of the Pacific cell (compare the blue and green curves in Fig. 2e, f). This shift can also be seen in the vertical wind at the 500 hPa level along the equator (Fig. 3): Over the East Indian Ocean and Maritime Continent the vertical wind decreases, whereas over the Pacific Ocean it increases. Thus an eastward shift of the Walker Circulation can be seen in the zonal stream function as well as in the vertical wind in both the CMIP3 and CMIP5 MMM change.

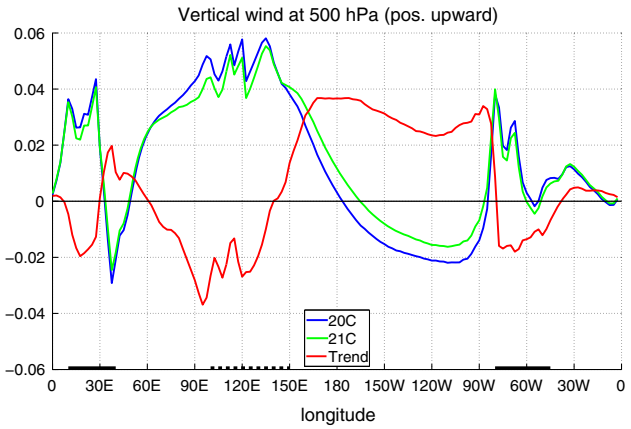

Fig. 3 Mean state of the vertical wind (positive upward) at 500 hPa, 5°S–5°N in 20C (*blue line*), 21C (*green line*) in Pa s^{-1} and trend over the period 1950–2099 in Pa s^{-1} (500 year)$^{-1}$ (*red dashed*) in CMIP5 MMM

The zero line of the stream function over the Maritime Continent warm pool region determines the western edge of the Pacific cell and coincides approximately with the maximum of convection (Fig. 3). This zero line shifts 6° to the east in the CMIP5 MMM and 8° in the CMIP3 MMM (Fig. 2e, f). Figure 4 shows the shift in the position of the western edge of the Pacific cell under global warming on the x-axis and the average trend in the box over the ascending branch of the Pacific and Indian Ocean cell on the y-axis (120°E–180°, 700–300 hPa) for each individual CMIP3 and CMIP5 model. Most models show a negative trend and an eastward shift under global warming. These two quantities appear to have a weak linear relation: models that tend to weaken most also tend to have a larger eastward shift.

4 East–west shift of the Walker Circulation during El Niño/La Niña

The centers of large scale convection and precipitation shift in the east–west direction during El Niño/La Niña events (e.g. Philander 1990). Whether the east–west shift of the convection during El Niño is associated with an east–west shift in the zonal circulation cells can be analysed using composites of the stream function for El Niño and La Niña events. As selection criteria for these composites we use the normalised Niño3.4 index (normalised with its standard deviation) from detrended SST anomalies. These

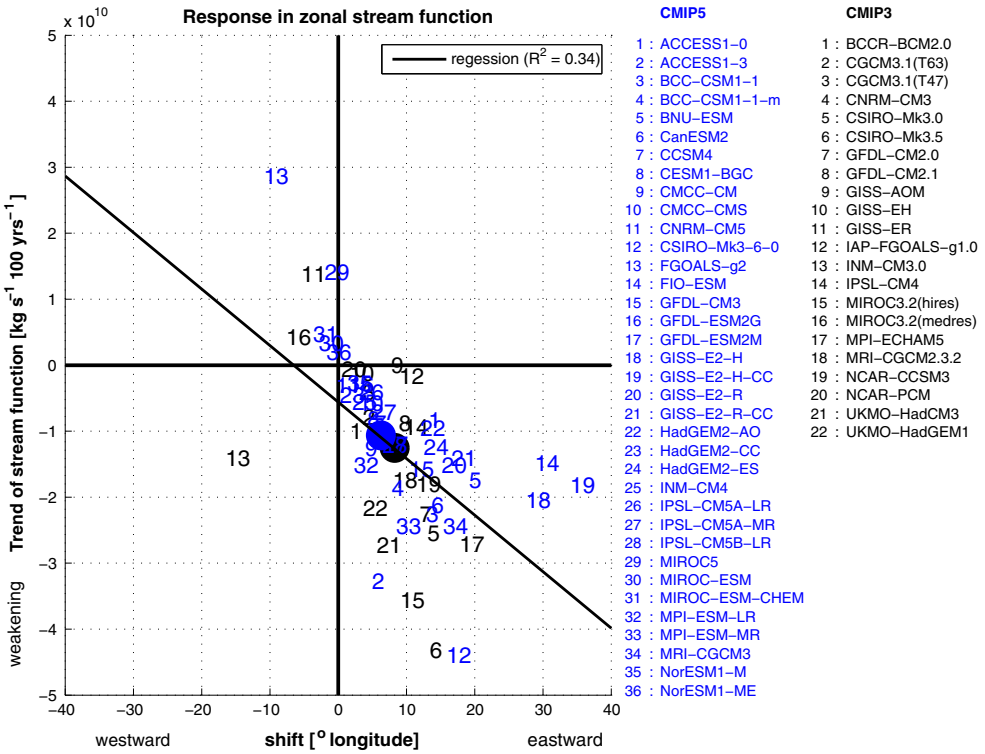

Fig. 4 Response of zonal stream function under global warming in the individual models of the CMIP3 and CMIP5 data base, on the x-axis the shift of the western edge (zero line of stream function) of Pacific cell, on the y-axis the trend of zonal stream function averaged over the box 120°E–180°, 700–300 hPa

composites contain all months with normalised Niño3.4 index > 1 for El Niño and normalised Niño3.4 index < -1 for La Niña.

The Walker Circulation in ERA Interim reanalysis data reveals an east–west shift in ENSO variability (Fig. 5a, b): The zonal circulation cells over the Indo-Pacific are considerably weaker during El Niño than during La Niña. Additionally, the western edge of the Walker Circulation shifts to the east of its mean state position during El Niño (176°E) and to the west during La Niña (140°E). Figure 5c shows the difference between the El Niño and La Niña composites. An interesting point is that ENSO affects not only the Pacific cell, but also has a significant impact on the circulation cell over the Indian Ocean.

Figure 5d–f shows the same composites as in Fig. 5a–c but for the CMIP5 MME over the period 1950–1979. Each model's standardised Niño3.4 index is used to select El Niño and La Niña events in each model. The western edge of the Pacific cell is at 141°E averaged across all years, 133°E during La Niña years, and at 165°E in El Niño years. This corresponds to a 32° difference between El Niño and La Niña years and is a very similar to the magnitude of the east–west shift evident in the reanalysis data. However, all three states are located roughly 10° further west in the models than they are in the reanalysis. The amplitude of the modelled ENSO variability (Fig. 5f) over the West Pacific is 30 % lower than it is in the reanalysis data.

It is interesting to note that the trend pattern from Fig. 2c, d has some similarities to the ENSO amplitude pattern in Fig. 5f. The pattern correlation coefficient is 0.61 in CMIP3 and 0.73 in CMIP5. This suggests that large parts of the trend under global warming might be linked to more El Niño-like conditions, as already seen in the trend of the box index of SST in Fig. 1. However, there is no linear relationship between the eastward shift during El Niño and the eastward shift under global warming in the individual models, i.e. models with a stronger eastward shift linked to ENSO variability do not show a stronger eastward shift under global warming (not shown).

From the similarity of the Walker Circulation response to ENSO and to global warming the question arises if they have the same mechanism. Figure 6a shows the vertical profile of the ENSO pattern (El Niño minus La Niña composite as in Fig. 5f) in the CMIP5 MME of atmospheric temperature along the equator. The strongest warming appears over the Pacific with a maximum at the surface and at 300 hPa. According to the two mechanisms mentioned in the introduction, we can decompose this pattern into a horizontal homogeneous and inhomogeneous part. Homogeneous warming, that increases with height,

acts to weaken the tropical circulations and an inhomogeneous warming may cause more ascending where it is relatively warm and more descending where it is relatively cold.

First, it is evident in Fig. 6b that ENSO is also associated with a homogeneous warming that increases with height. Figure 6c indicates that variability in the zonal stream function associated with ENSO (contours) fits quite well to the inhomogeneous warming (shading). This is evident because additional ascending occurs where the atmospheric warming is stronger and additional descending where the atmosphere warms less. In ENSO the homogeneous part is of the same order as the inhomogeneous (Fig. 6b, c).

Under global warming (Fig. 6d–f) the homogeneous and inhomogeneous warming have a similar structure as in the ENSO composite: both show the strongest warming near the 300 hPa level in the homogeneous warming and in the inhomogeneous warming a stronger warming over the East and Central Pacific than over the East Indian Ocean and Maritime Continent in the levels below 200 hPa and vice versa above. But under global warming the homogeneous warming is roughly 10 times larger than the inhomogeneous warming, over the full time period as well as on shorter time scales. Here the response of zonal stream function (contours in Fig. 6f) only roughly fits to the inhomogeneous warming (shading in Fig. 6f), strongest disagreeing over the Maritime Continent.

5 Asymmetry in the response of the Walker Circulation during El Niño/La Niña

Here we determine whether or not the Walker Circulation exhibits a spatial asymmetry in ENSO variability as one can find in SST (e.g. Dommenget et al. 2013). We repeat the composite analysis described above, but now with detrended anomalies instead of the full field values of the zonal stream function. Additionally we normalised each composite with its mean Niño3.4 index (e.g. for El Niño: mean (Niño3.4 > 1)) to account for the skewness of SST. In reanalysis data we get anomalous ascent over the West Indian Ocean and Central Pacific and anomalous descent over most of the Maritime Continent region (between 60°E and 160°E) during El Niño (Fig. 7a). The opposite is approximately true during La Niña events (Fig. 7b, note the reversed sign), though anomalies are shifted more to the west and they tend to be lower in magnitude. These east–west asymmetries in location and strength represent a non-linearity. Figure 7c shows the sum of El Nino and La

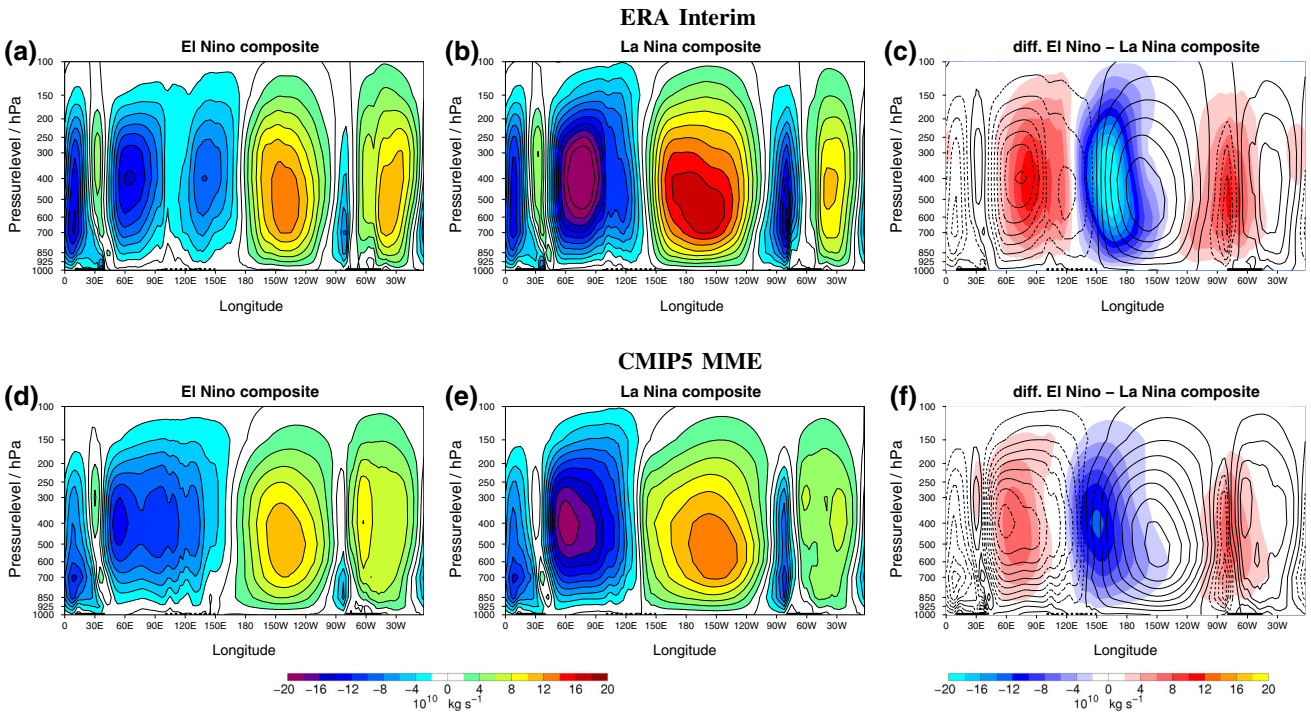

Fig. 5 Composites of zonal stream function **a–c** in ERA Interim, with normalised Niño3.4 index (170°W–120°W, 5°S–5°N) as selection criterion, **a** for Niño3.4 > 1 (El Niño), **b** for Niño3.4 < −1 (La Niña), **c** *shading* difference El Niño–La Niña (i.e. ENSO amplitude), contours: climatological mean in ERA Interim over the period 1979–2012; **d–f** same as **a–c** but here for CMIP5 MME in 20C

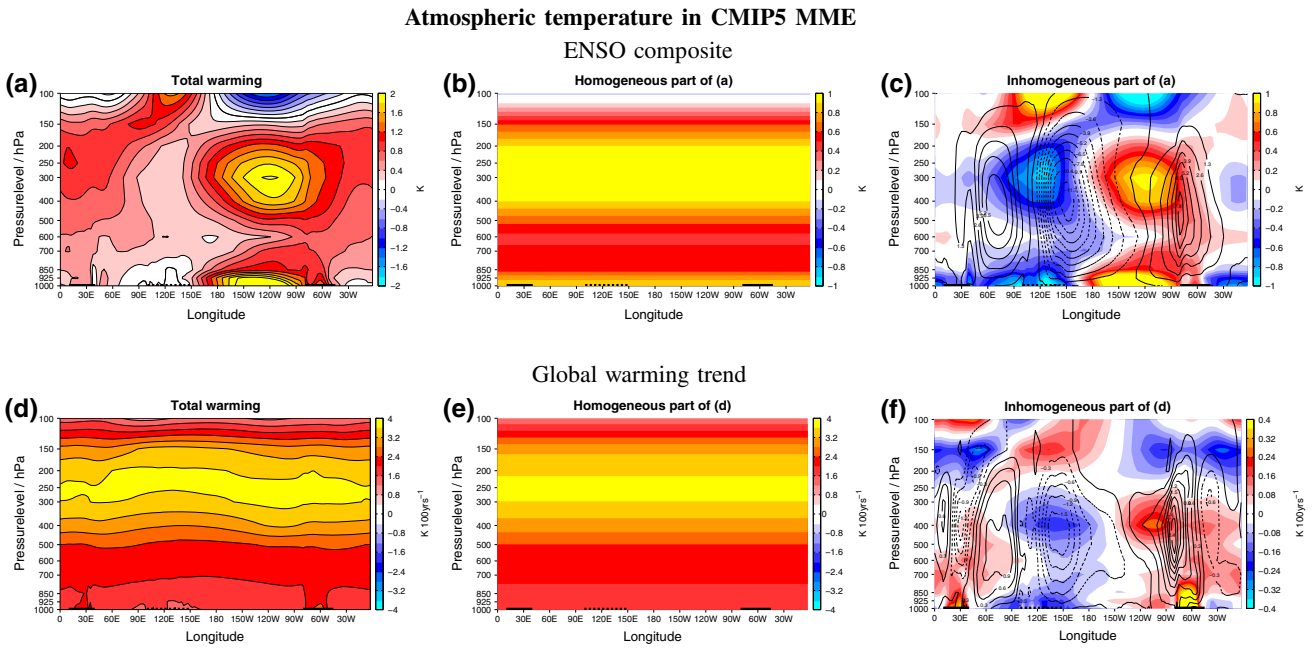

Fig. 6 **a** Same as Fig. 5f, but here for atmospheric temperature in the CMIP5 MME (i.e. the atmospheric warming in an El Niño–La Niña composite), **b** horizontal homogeneous warming (zonal mean of **a**), **c** *shading* horizontal inhomogeneous warming **a** minus **b**, contours: ENSO amplitude from Fig. 5f, **d** linear trend of atmospheric temperature over the period from 1950 till 2099 in the CMIP5 MMM, **e**, **f** same as **b**, **c**, but here for **d**, but in **f** the trend pattern of Fig. 2d as contours

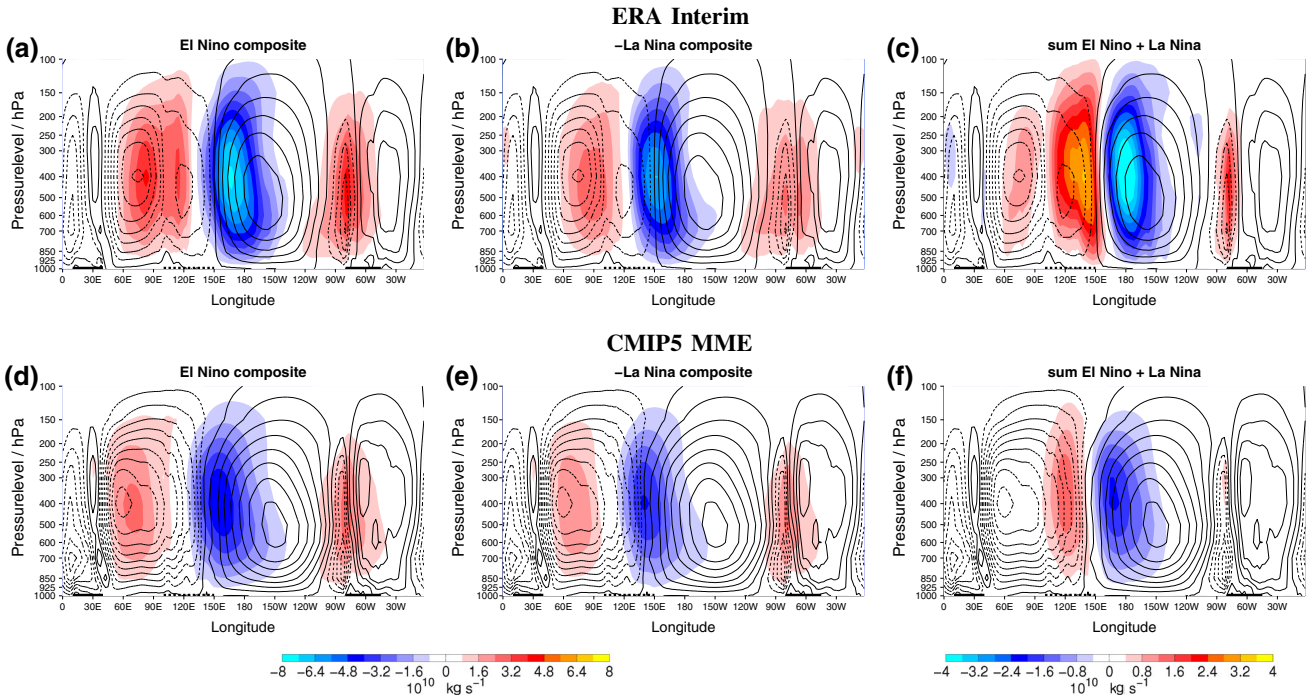

Fig. 7 Same as Fig. 5, but here composites of detrended anomalies, normalised with mean Niño3.4 index (170°W–120°W, 5°S–5°N), *shading* **a** for Niño3.4 > 1 (El Niño), **b** for Niño3.4 < -1 (La Niña), **c** sum El Niño + La Niña (i.e. a measure for the non-linearity); contours in figures **a**–**c**: climatological mean in ERA Interim over the period 1979–2012; **d**–**f** same as **a**–**c** but here for CMIP5 MME in 20C

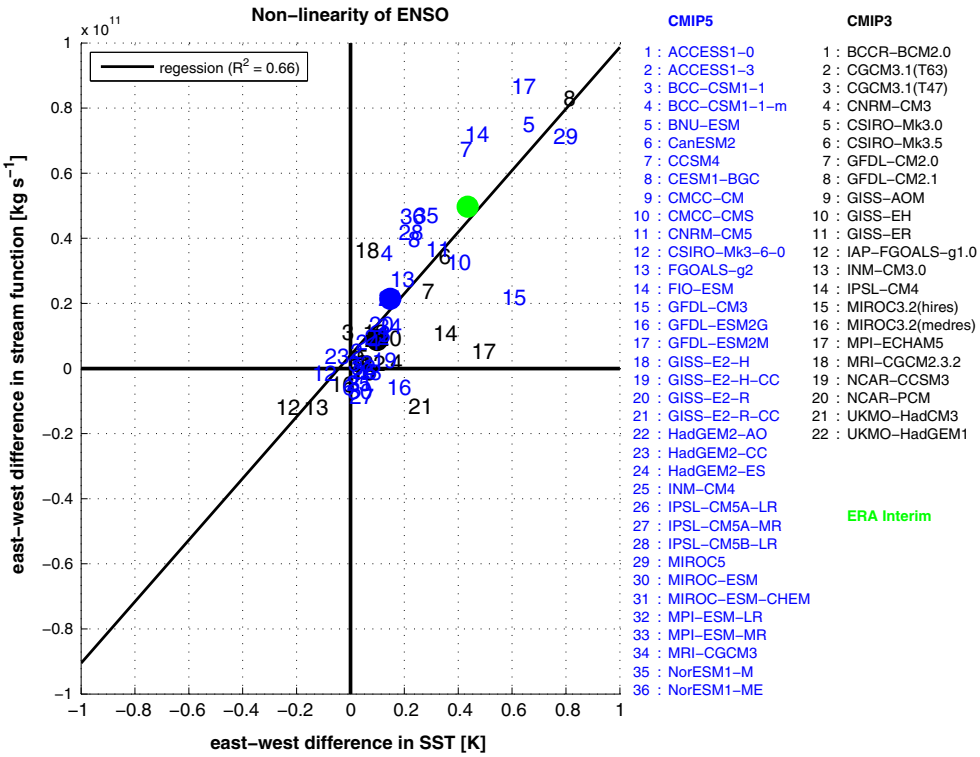

Fig. 8 Non-linearity of ENSO in the individual models of CMIP3 and CMIP5 data base and ERA Interim, on the x-axis a measure of the non-linearity of the SST: the difference of eastern box (80°W–140°W, 5°S–5°N) and western box (140°E–160°W, 5°S–5°N) of the sum of El Niño and La Niña composites (as defined in Dommenget et al. 2013); on the y-axis a measure of the non-linearity of the zonal stream function: the difference of western box (120°E–150°E, 700–200 hPa) and eastern box (170°E–160°W, 700–200 hPa) of the sum of El Niño and La Niña composites, like in Fig. 7c

Nina composite. The amplitude in this figure indicates the regions where the variability of the Walker Circulation linked to ENSO is non-linear, as in a linear case the sum of El Niño and La Niña composite would be zero due to the use of anomalies and the normalisation by the mean Niño3.4 index. The zonal circulation cells anomalies over most of the Indo-Pacific region are non-linear, with a maximum between 110°E and 140°W.

The composites of the CMIP5 MME over the period 1950-1979 (Fig. 7d–f) are very similar to the composites of reanalysis data (Fig. 7a–c). The modelled La Niña response also tends to be displaced west of the modeled El Niño response, and the modeled La Niña response tends to be smaller in amplitude than the modeled El Niño response. The modeled ENSO non-linearity is, however, confined to a smaller region (110°E–140°W; see Fig. 7f) and has weaker magnitude than their counterparts in the reanalysis data. In order to quantify how well the MME and the individual climate models simulate the spatial non-linearity of the Walker Circulation, we define a simple two box index: The west-east difference between a western box (120°E–150°E, 200–700 hPa) and eastern box (170°E–160°W, 200–700 hPa) in the difference plot of the composites as shown for reanalysis data in Fig. 7c. We can compare this with a measure for the spatial non-linearity of ENSO in SST, as defined in Dommenget et al. (2013): As for the stream function, we calculate for SST the east–west difference between an eastern box (80°W–140°W, 5°S–5°N) and a western box (140°E–160°W, 5°S–5°N) of the sum of normalised El Niño and La Niña composites. Figure 8 shows these two measures for ERA Interim reanalysis data (1979–2012) and all climate models of the CMIP3 and CMIP5 data base for the period 1900–1999. The MMEs of CMIP3 and CMIP5 both have a much weaker non-linearity than ERA Interim, but CMIP5 is closer to the observed than CMIP3. From the individual models we can see two interesting features: First, most of the models have problems in simulating a realistic non-linearity (cluster of models around zero). Second, from the strong linear relationship we can see that the skill in simulating a strong non-linearity in SST seems to be related to the skill in simulating a strong non-linearity in the zonal stream function. We cannot say from this analysis if the non-linearity of the SST is caused by the non-linearity of the atmosphere or vice versa. But in a recent study, Frauen and Dommenget (2010) found that non-linear atmospheric feedbacks linked to ENSO variability can exist with a linear ocean, indicating that the atmosphere alone can cause substantial ENSO non-linearity.

6 Changes in the modes of variability in response to global warming

We now analyse the changes in the modes of variability under global warming. We will base this on Empirical

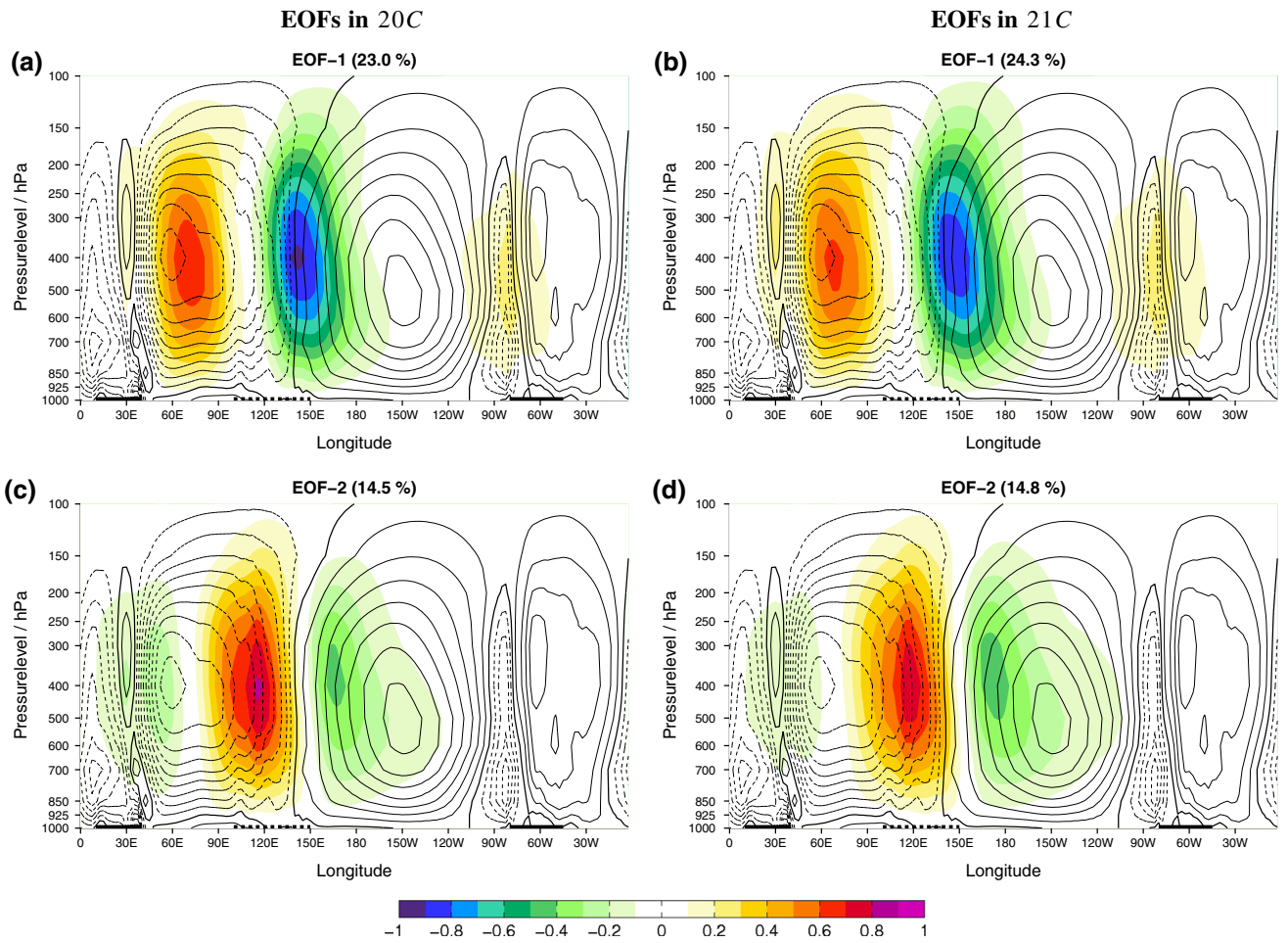

Fig. 9 EOFs of zonal stream function in CMIP5 MME, *shading* **a** EOF-1 in 20C, **b** EOF-1 in 21C, **c** EOF-2 in 20C, **d** EOF-2 in 21C, explained variance is given in the *header* in *brackets* respectively; contours in all figures: mean state in 20C from Fig. 2b

Orthogonal Function (EOF) analysis, which is a common way to determine the modes of variability. We will focus on two questions: Do the EOF–patterns change and thus indicate changes in the spatial patterns of variability? Second, do the principal component (PC) time series of the leading modes have a long-term trend under global warming? If yes, this would indicate that the trend-pattern may be related to leading modes of internal variability.

For the first question we will closely examine the EOF patterns in the CMIP5 MME in the two time periods 1950–1979 (20C) and 2070–2099 (21C). For EOF analysis we concatenate the monthly data of the individual climate models to one long data set of 36 × 30 years = 1,080 - years for CMIP5 (22 × 30 years = 660 years for CMIP3, results not shown) for each time period 20C and 21C, where detrended anomalies are defined for each model individually first. The EOF-1 patterns (Fig. 9a, b) over these periods are very similar to the composite of El Niño and La Niña (Fig. 7d, e). They are also similar to the combined EOF-1 of zonal stream function and SST, where the SST pattern is the typical ENSO pattern (e.g. Kang and Kug 2002, not shown). Thus the EOF-1 is associated with ENSO variability in zonal stream function and describes an east–west shift of the edge between the Indian and Pacific cell. The western Pacific pole of EOF-1 is further east in 21C and this pole becomes a bit weaker than during 20C. EOF-2 describes a strengthening or weakening of the eastern part of Indian cell and the western part of the Pacific cell and also shifts a little bit to the east in 21C.

For a more detailed analysis of the spatial changes we can use Distinct Empirical Orthogonal Function (DEOF) analysis as described by Bayr and Dommenget (2013b). This method compares all the leading modes of variability in two data sets on the basis of the multi-variate EOF patterns and finds the patterns of the largest changes in variability. In DEOF analysis the two EOF sets from 20C and 21C are compared with each other via projecting one set of EOF patterns onto the other to find the pattern that has the largest

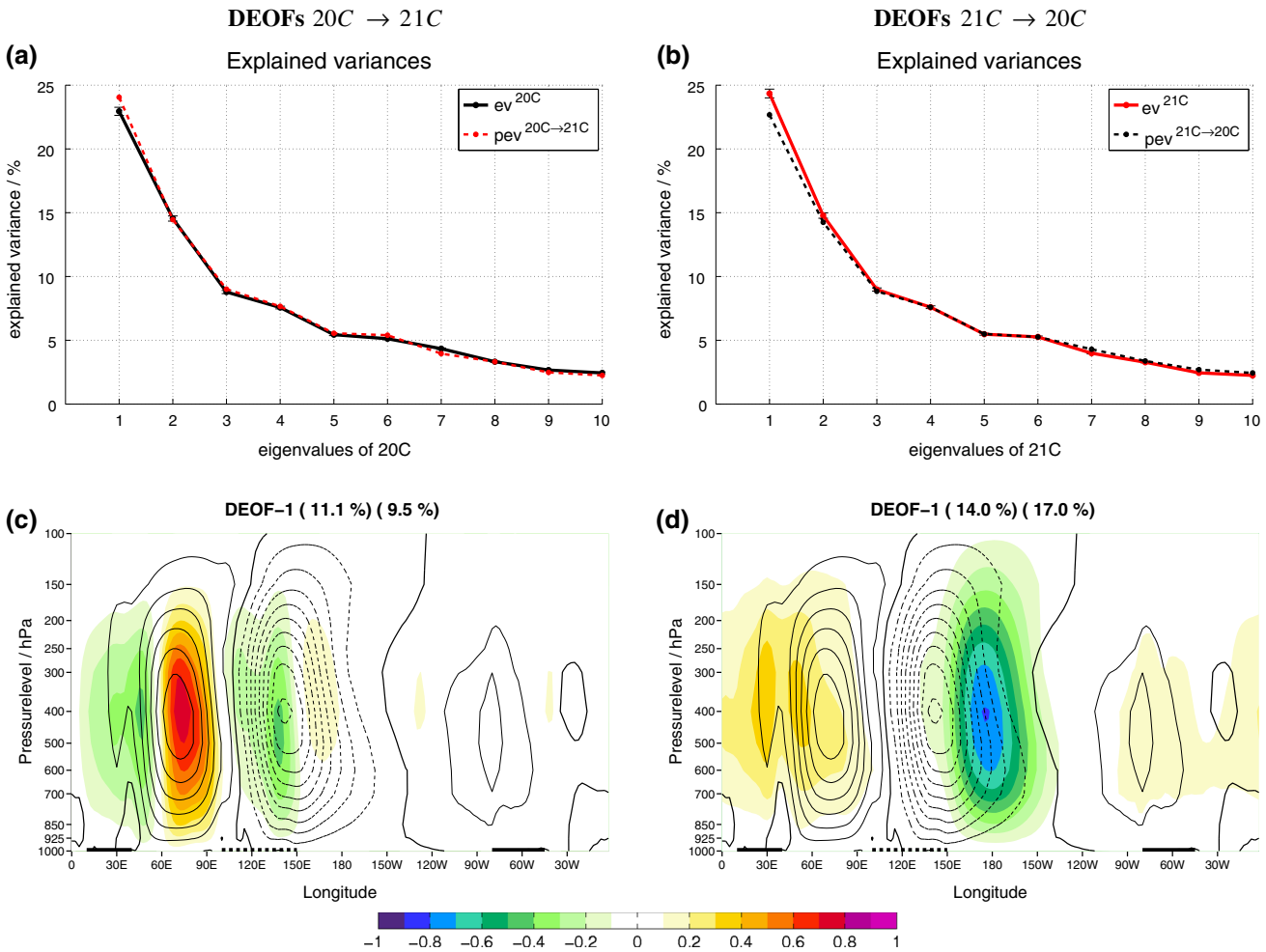

Fig. 10 **a** Explained variances of the eigenvalues in 20C (*black solid line*) and explained variances of 20C projected onto the eigenvalues of 21C (*red dashed line*), the *error bars* show the statistical uncertainties of the explained variances due to sampling errors according to North et al. (1982); **b** same as **a**, but here for the eigenvalues of 21C (*red solid line*) and the explained variances of 21C projected onto the eigenvalues of 20C (*black dashed line*), **c** DEOF$^{20C\rightarrow 21C}$ pattern; the values given in the header in brackets is the explained variance of this pattern in 20C and 21C, respectively, **d** as **c**, but here DEOF$^{21C\rightarrow 20C}$ pattern; contours in **c**–**d**: EOF-1 in 20C from Fig. 9a

difference in explained variance in these two sets of EOF pattern (see Bayr and Dommenget (2013b) for further details). The projected explained variances (Fig. 10a, b) show both that the variability becomes more large scale under global warming as the leading modes of variability have a lower explained variance in 20C than they do in 21C. This means that fewer modes are needed in 21C to explain the largest part of the variance (The spatial degrees of freedom from Bretherton et al. (1999) decrease from 10.2 in 20C to 9.5 in 21C). Additionally, EOF-1 has the largest difference in terms of explained variance in the two data sets.

The projection of the EOFs of 20C onto the EOFs of 21C (DEOF-1$^{20C\rightarrow 21C}$) maximizes the explained variance differences between 20C and 21C. It is the pattern that loses the largest amount of variance in 21C relative to 20C. The DEOF-1$^{20C\rightarrow 21C}$ (Fig. 10c) mainly shows that the variance in the Indian Ocean cell is reduced by 14 % in 21C relative to its 20C value (a change in explained variance from 11.1 to 9.5 %). The DEOF-1$^{21C\rightarrow 20C}$ maximizes the explained variance differences between 21C and 20C. It is the pattern that gains the largest amount of variance in 21C relative to 20C. The DEOF-1$^{21C\rightarrow 20C}$ (Fig. 10d) mainly shows that the variance in the central Pacific pole has increased by 21 % in 21C relative to its 20C value (a change in explained variance from 14.0 to 17.0 %). Combined the two leading DEOF-modes indicate a shift in the variability from the Indian Ocean into the

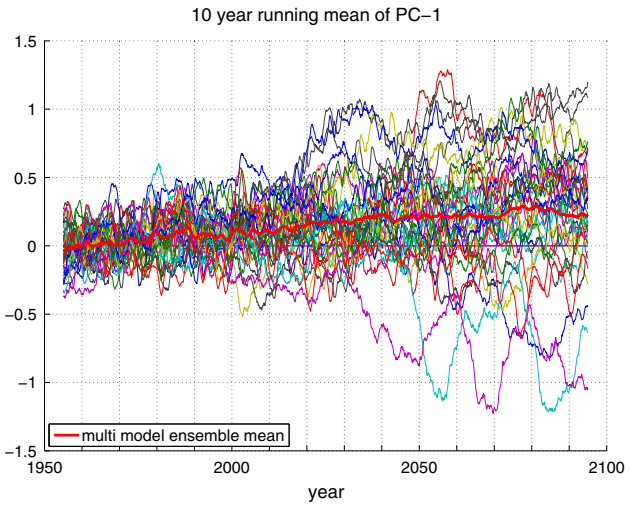

Fig. 11 10 year running mean of PC-1 of zonal stream function in all individual CMIP5 models; the *thick red line* is the average of all 36 individual models

central Pacific in EOF-1. DEOF-$1^{20C\rightarrow 21C}$ is also of smaller spatial scale (e.g. distance between the main poles) than DEOF-$1^{21C\rightarrow 20C}$. This again suggests that the variability in 21C tends towards larger scales.

This shift from the Indian into the Pacific Ocean is consistent with the spatial non-linearity discussed in Sect. 5. The El Niño composite pattern in zonal stream function is further east than the La Niña composite pattern, thus an eastward shift of the dominant mode of variability can be linked to a shift towards more El Niño-like conditions.

Next we have a look at the long-term trend in the PC time series. We therefore use the EOF-1 pattern of 20C and calculate for each model individually the PC timeseries for this pattern over the period from 1950 to 2099, from anomalies relative to the climatology of the period from 1950 to 1979. The similarity of the trend pattern in Fig. 2d with EOF-1 from Fig. 9a, b is already a strong hint that the zonal circulation shifts in its dominant mode of variability towards more El Niño-like conditions. Indeed a positive trend in PC-1 (El Niño-like) can be seen in the average over all CMIP5 models (red line in Fig. 11), with the strongest trend in the first half of the 21C and only a weak trend in the second half of the 21C, consistent with the radiative forcing and warming in the RCP4.5 scenario. But the decadal (natural) variability of the individual models is still much larger than the trend in the MMM, indicating that detection of a Walker Circulation trend due to increased greenhouse gases will be very difficult in the next decades, if we are not able to separate the climate change signal from internal variability. No other PC time series exhibit a strong trend in the MME.

Finally we want to find out how much of the global warming trend from Fig. 2c, d is related to the trend in the dominant mode of variability. In each individual model we can remove the variability and trend associated with the EOF-1 pattern. After removing EOF-1 in each model individually we can calculate a new MMM and the residual trend of this new MMM (Fig. 12). Much of the trend has vanished over the Indo-Pacific region and the trend in PC-1 can explain 52 % of the trend in CMIP5 over the entire tropics or 69 % of the Walker Circulation changes (49 and 67 % in CMIP3, respectively). The residual trend pattern shows a reduction of convection over Africa and South America, consistent with the general weakening as found by Vecchi and Soden (2007), less descending over the cold tongue region, consistent with the strong warming there, and an upward expansion the Indian and Pacific cell, consistent with the results of Haarsma and Selten (2012) and Singh and O'Gorman (2012).

7 Recent trends in ERA Interim reanalysis data

In this section we examine trends in the observed zonal circulation over the last three decades. We have to keep in mind that in comparison to simulated trends the observed trend has a lower signal to noise ratio due to the shorter time period and a stronger influence of natural variability as it is only one realization, whereas the CMIP MMM change includes many realizations. Thus the observed trends might contain a larger fraction of natural variability than the CMIP MMM trend.

The trend pattern over the Pacific for the period 1979 until 2012 is mostly the opposite of the CMIP trend pattern (compare Fig. 13a with Fig. 2c, d): it shows a westward shift of the western edge and a strengthening of the Walker Circulation (see also Fig. 13c). The trend has a magnitude that is roughly 10 times larger than in the CMIP MMM. The pattern again has a high pattern correlation coefficient with the dominant mode of variability (−0.70), thus indicating that the Walker Circulation shifted towards more La Niña-like conditions over the period analysed. As in the CMIP models, the trend in EOF-1 explains 49 % of the trend over the entire tropics and even 75 % over the Pacific (Fig. 13b). The residual trend shows a strong increase of convection over South America in the last decades. From the time series of EOF-1 of zonal stream function in Fig. 13d we can see that there was a strong inter-decadal fluctuation of ENSO in the last decades, with more and stronger El Niño's in the time period 1979 till 1998 and more and stronger La Niña's in the time period 1999 till 2012, as also stated by Kosaka and Xie (2013). Thus, although the sign of the trends in reanalysis data is opposite to that of the simulated global warming trend in the CMIP models, the trend of the dominant mode of variability again plays a crucial role for the trend in the Walker Circulation.

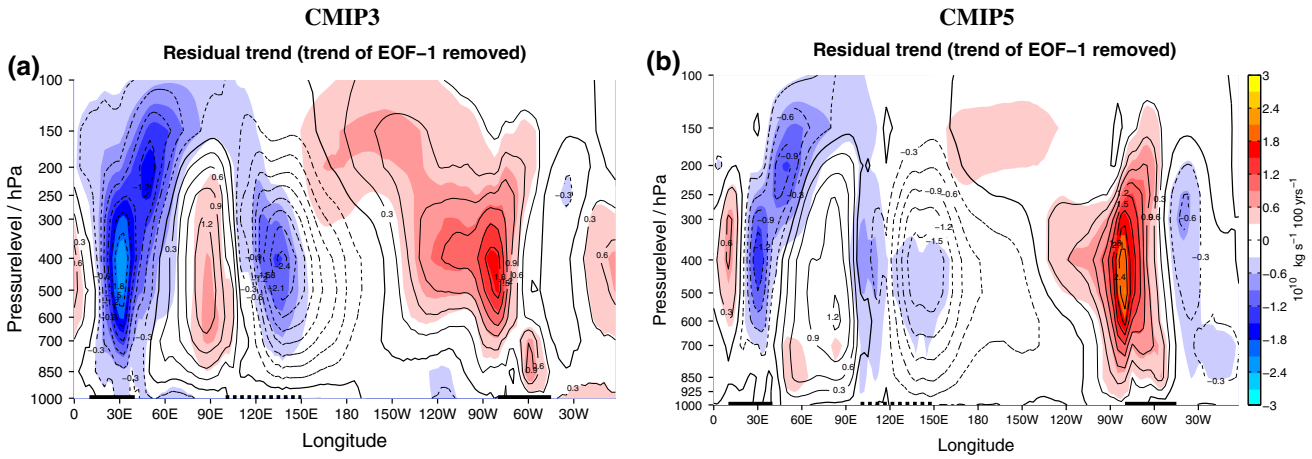

Fig. 12 **a** *Shading* residual trend in zonal stream function in CMIP3 MMM after removing the trend of EOF-1 in each model individually, contours: trend in stream function from Fig. 2c (before removing the trend of EOF-1) for comparison, **b** same as **a** but here for CMIP5 MMM

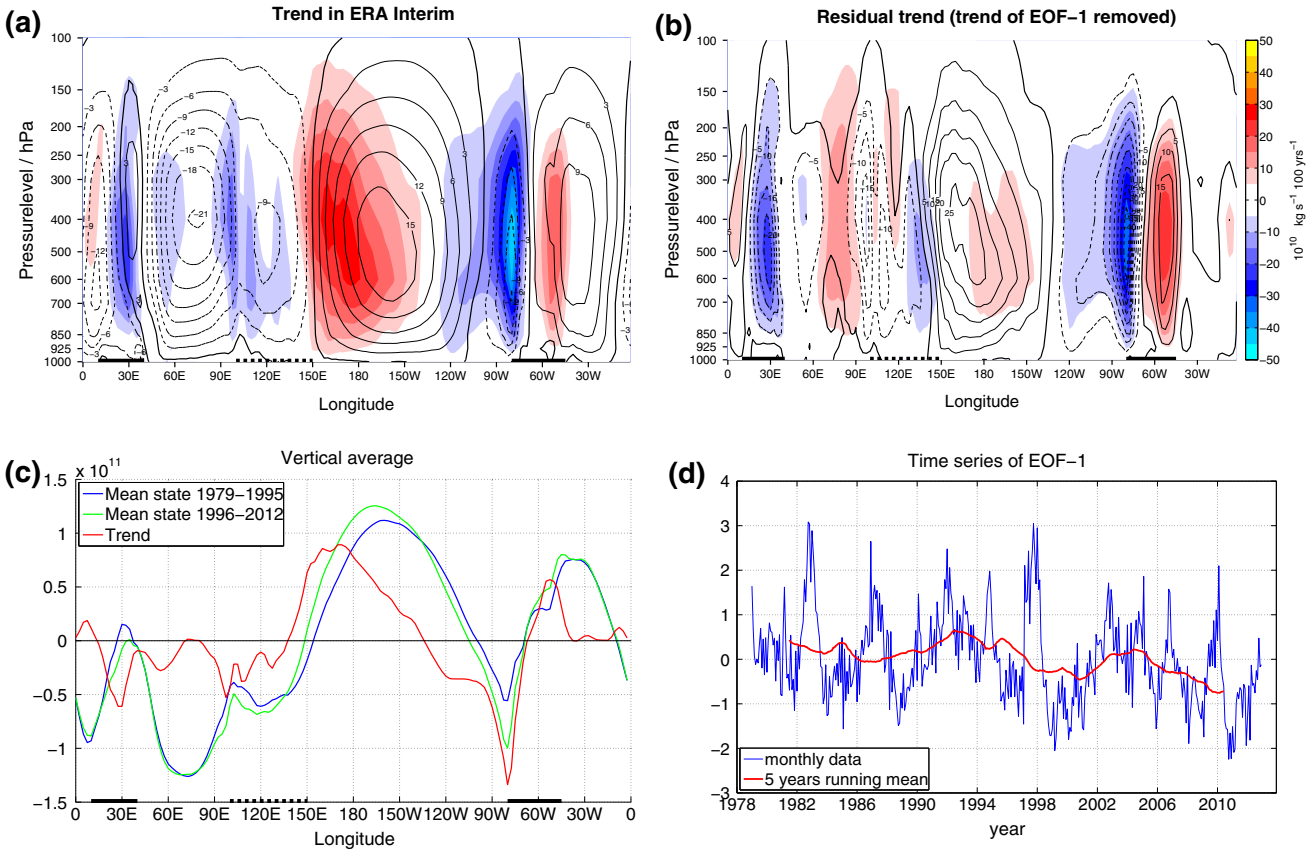

Fig. 13 **a** Same as Fig. 2c, but here the trend in ERA Interim over the period 1979–2012, climatological mean of ERA Interim over this period as contours, **b** *shading* the residual trend in ERA Interim after removing trend of EOF-1, contours: the trend of **a**, **c** same as Fig. 2e, f, but here for mean state (in kg s^{-1}) and trend (in kg s^{-1} (50 year)$^{-1}$) in ERA Interim, **d** time series of EOF-1 of zonal stream function in ERA Interim

8 Relation of stream function and SLP

An open question is the relation of our results based on zonal stream function to the results of previous studies using SLP. Figure 14 shows the meridional average (5°S–5°N) of SLP and vertical wind at the 500 hPa level, the vertical and meridional mean of tropospheric temperature (T_{tropos}) and the zonal gradient of vertical and meridional

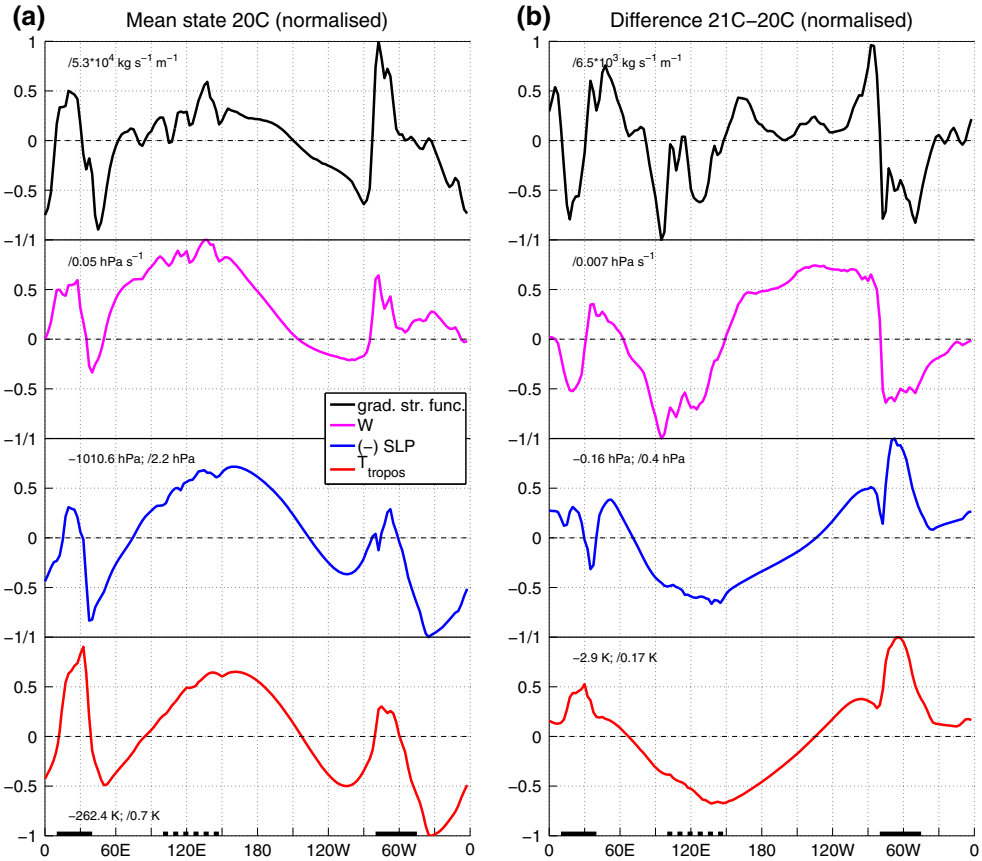

Fig. 14 Meridional average (5°S–5°N) of SLP and vertical wind (W) at the 500 hPa level, the vertical and meridional mean of tropospheric temperature (T_{tropos}, as defined in Bayr and Dommenget 2013a) and the zonal gradient of vertical and meridional averaged zonal stream function in the CMIP5 MMM, zonal mean for SLP and T_{tropos} removed and all variables are normalised (values are shown in the figure); **a** mean state in 20C, **b** difference 21C–20C

averaged zonal stream function in the CMIP5 MMM. For a better comparison we removed the area means for SLP and T_{tropos} and all variables are normalised.

In the mean state (Fig. 14a) we see good agreement between all four variables: Convection takes place were the temperatures are high (the three 'heat sources' Africa, Maritime Continent and South America), SLP is low and the stream function gradients are large. However, this general agreement is not seen in the changes 21C to 20C (Fig. 14b). The change in vertical wind again agrees with the zonal gradient of the zonal stream function (correlation 0.74) and the T_{tropos} and SLP response are very similar (correlation −0.94), as already found in Bayr and Dommenget (2013a). But over most regions the changes in stream function and vertical wind do not agree with the changes in SLP and T_{tropos}, especially over Africa and South America. Here the land-sea warming contrast reduces the SLP according to Bayr and Dommenget (2013a), which would suggest an increase in convection. In contrast, the vertical wind and the stream function show more descending. There is no explanation for this discrepancy yet, but it indicates that changes in SLP cannot reveal the full picture of changes over the entire troposphere, like convection and associated precipitation patterns. Further investigation is needed to better understand the causes of these discrepancies.

9 Summary and discussion

The main purpose of this study is to analyze the response of the zonal circulation cells (with a special focus on the Walker Circulation) to global warming and its relation to ENSO using the last two generations of climate models. The focus is on the eastward shift of the Walker Circulation and the changes in the modes of variability. We choose the zonal stream function for this analysis, as it is a direct representation of the zonal circulation and also available over all levels of the troposphere. We find that the trend patterns of the zonal circulation under global warming (Fig. 2c, d) are very similar in the two CMIP MMMs, despite the differences in models, resolution, ensemble size and emission scenario. This underlines the robustness of the signal. The trend pattern shows more ascending air over the West Indian Ocean, Central and East Pacific, and more descending air over the three main convection regions Africa, the Maritime Continent and South America, thus a weakening of the zonal circulations. Additionally there are substantial eastward shifts in the western part of the Walker Circulations in both the CMIP5 and CMIP3 models of 6° and 8° respectively.

The MMM trend patterns exhibit some similarity to the patterns associated with internally generated ENSO variability of the zonal stream function. Indeed a large part of

the global warming response corresponds to a shift towards more El Niño-like conditions. The El Niño-like trend in zonal stream function will cause that neutral ENSO conditions at the end of the 21C resemble El Niño conditions, if referred to the 20C climate. How El Niño-like the global warming trend is in comparison with an average El Niño can be calculated: An average El Niño in the CMIP5 MME is associated with an amplitude of -3.6×10^{-10} kg s^{-1} in the box (120°E–180°, 700–300 hPa) as defined for Fig. 4 and an eastward shift of 25° longitude. Thus a global warming trend of the same size would mean a 100 % shift towards an average El Niño, with 20C as reference climate. The eastward shift of 6° and the trend of -1.1×10^{10} kg s^{-1} (100 year^{-1}) in the CMIP5 MMM in this box (Fig. 4) would thus mean a long-term shift of 30 % in amplitude and 26 % in location towards an average El Niño event over the next century (31 and 37 % in CMIP3, respectively).

Further we could show that the internal variability of the zonal stream function exhibits a substantial spatial non-linearity, as the El Niño anomaly pattern of the zonal stream function is more in the east than the La Niña anomaly pattern. The spatial non-linearity in the zonal stream function is linear related to the non-linearity of ENSO in SST in the individual models. However, most models have problems in simulating a realistic ENSO non-linearity in both variables, subsequently the non-linearity of the CMIP MME is less than half as strong as in the ERA Interim reanalysis data.

The similarity of the eastward shift in the zonal stream function during global warming and strong El Niño events may indicate a common forcing mechanism for these shifts. Several studies have shown that the ENSO non-linearity is caused by the atmospheric response to SST anomalies (Kang and Kug 2002; Philip and van Oldenborgh 2009; Frauen and Dommenget 2010), in particular the eastward shift of strong El Niño events (Dommenget et al. 2013). Thus the atmosphere responds with an eastward shift to SST warming. Under global warming the enhanced hydrological cycle to first order leads to a horizontally homogenous but vertically enhanced warming. This warming trend is also associated with an eastward shift, indicating that horizontally homogenous and vertically enhanced warming patterns, as in both global warming trend and during El Niño, may induce an eastward shift of the zonal circulation cell over the Pacific.

The prominent changes in the modes of variability under global warming are an eastward shift from the Indian Ocean to the central Pacific of EOF-1 and a shift towards larger scale variability. EOF-1 is associated with ENSO variability and has a positive (El Niño-like) trend under global warming. After removing the trend associated with EOF-1, two-third of the trends vanishes over the Pacific, i.e. are related to more El Niño-like conditions.

Most of the individual climate models predict a weakening and an eastward shift of the Walker Circulation under global warming. However a minority of models show no significant trends and some even predict a strengthening and westward shift. This indicates that the homogeneous warming, which can only weaken the Walker Circulation in a warmer climate, can't be the dominant mechanism in all climate models. The inhomogeneous warming seems to be the dominant mechanism in the models with a strengthening Walker Circulation, as this mechanism can act in general in both directions, either weakening or strengthening the Walker Circulation.

In the ERA Interim reanalysis data we found a strengthening of the Walker Circulation and westward shift over the last three decades. In recent literature there is a debate about the changes of the Walker Circulation over the last decades: Analysing observations and model runs forced with observed SST and/or greenhouse gas concentrations the studies of Sohn and Park (2010), Meng et al. (2011), Luo et al. (2012) and L'Heureux et al. (2013) found a strengthening of the Walker Circulation. These studies explain the strengthening with a more La Niña-like SST warming or a stronger warming over the Indian Ocean than over the Pacific over the last decades. But several other studies found a weakening of the Walker Circulation over much longer periods (Vecchi et al. 2006; Power and Kociuba 2010; Yu and Zwiers 2010; Tokinaga et al. 2012a, b; DiNezio et al. 2013), consistent with the homogeneous warming mechanism mentioned in the introduction. A recent study by Solomon and Newman (2012) found out that there are large discrepancies in the SST trends over the Indo-Pacific in the different observed data sets, which are caused by different representations of El Niño in these observed data sets. A second problem is the distinction between externally forced trends and internal variability in relative short records, so that Power and Kociuba (2011) conclude, that external forcing accounts for 30–70 % of the observed Walker Circulation changes over the entire 20C, with internal variability making up the rest. To sum up: due to relative short records it is difficult to say what part of the trend in ERA Interim reanalysis data is caused by global warming, by natural variability or even is just a measure uncertainty.

With the opposite direction between the predicted trend in the CMIP MMMs and the trends of the recent decades in ERA Interim, there are two conclusions possible: One conclusion could be that the trend in ERA Interim is mostly due to increased greenhouse gases and the CMIP MMMs predict the wrong sign of the forced response. The other conclusion is that the trends in ERA Interim are dominated by natural decadal variations of ENSO variability and that under global warming the Walker Circulation will shift

eastward and weaken, as the CMIP models predict. We think this latter explanation is quite likely, as both CMIP MMMs predict it and the dominant mode of variability exhibits strong decadal trends in Fig. 11. Nevertheless, both possible conclusions have one important thing in common: a large part of the Walker Circulation trend follows a pre-existing mode of variability, thus can be described to some extend as more El Niño-like or more La Niña-like. We have to keep in mind that the ENSO response of the climate models under global warming is still quite uncertain (e.g. Latif and Keenlyside 2009), but the MMMs of climate models carried out for the IPCC AR4 and AR5 predict a more El Niño-like response and therefore an eastward shift and weakening of the Walker Circulation in future climate.

Acknowledgments We acknowledge the World Climate Research Program's Working Group on Coupled Modeling, the individual modeling groups of the Climate Model Intercomparison Project (CMIP3 and CMIP5) and ECMWF for providing the data sets. This work was supported by the Deutsche Forschungsgemeinschaft (DFG) through project DO1038/5-1, the ARC Centre of Excellence in Climate System Science (CE110001028), the ARC project "Beyond the linear dynamics of the El Nino Southern Oscillation" (DP120101442), the RACE Project of BMBF, the NACLIM Project of the European Union and the Australian Climate Change Science Program. We thank Hanh Nguyen for providing the code to calculate the zonal stream function and Hardi Bordbar, Sabine Haase and the anonymous reviewers for discussion and useful comments.

References

Bayr T, Dommenget D (2013a) The tropospheric land-sea warming contrast as the driver of tropical sea level pressure changes. J Clim 26:1387–1402. doi:10.1175/JCLI-D-11-00731.1

Bayr T, Dommenget D (2013b) Comparing the spatial structure of variability in two datasets against each other on the basis of EOF-modes. Clim Dyn. doi:10.1007/s00382-013-1708-x

Bengtsson L, Hodges KI (2009) On the evaluation of temperature trends in the tropical troposphere. Clim Dyn 36:419–430. doi:10.1007/s00382-009-0680-y

Bretherton CS, Widmann M, Dymnikov VP, Wallace JM, Bladé I (1999) The effective number of spatial degrees of freedom of a time-varying field. J Clim 12:1990–2009

Clement AC, Seager R, Cane MA, Zebiak SE (1996) An ocean dynamical thermostat. J Clim 9:2190–2196

DiNezio PN, Clement AC, Vecchi GA, Soden BJ, Kirtman BP, Lee S-K (2009) Climate response of the equatorial pacific to global warming. J Clim 22:4873–4892. doi:10.1175/2009JCLI2982.1

DiNezio PN, Clement A, Vecchi GA, Soden B, Broccoli AJ, Otto-Bliesner BL, Braconnot P (2011) The response of the Walker circulation to Last Glacial Maximum forcing: Implications for detection in proxies. Paleoceanography 26. doi:10.1029/2010PA002083

DiNezio PN, Vecchi GA, Clement AC (2013) Detectability of changes in the Walker circulation in response to global warming. J Clim 130114154537002, doi:10.1175/JCLI-D-12-00531.1

Dommenget D, Bayr T, Frauen C (2013) Analysis of the non-linearity in the pattern and time evolution of El Niño southern oscillation. Clim Dyn 40:2825–2847. doi:10.1007/s00382-012-1475-0

Frauen C, Dommenget D (2010) El Niño and La Niña amplitude asymmetry caused by atmospheric feedbacks. Geophys Res Lett 37:L18801. doi:10.1029/2010GL044444

Haarsma RJ, Selten F (2012) Anthropogenic changes in the Walker circulation and their impact on the extra-tropical planetary wave structure in the Northern Hemisphere. Clim Dyn. doi:10.1007/s00382-012-1308-1

Hastenrath S (1985) Climate and circulation of the tropics. D. Reisel Publishing Company, Dordrecht

Held IM, Soden BJ (2006) Robust responses of the hydrological cycle to global warming. J Clim 19:5686–5699. doi:10.1175/JCLI3990.1

Hoerling MP, Kumar A, Zhong M (1997) El Niño, La Niña, and the nonlinearity of their teleconnections. J Clim 10:1769–1786. doi:10.1175/1520-0442(1997)010<1769:ENOLNA>2.0.CO;2

Kang I-S, Kug J-S (2002) El Niño and La Niña sea surface temperature anomalies: asymmetry characteristics associated with their wind stress anomalies. J Geophys Res 107:4372. doi:10.1029/2001JD000393

Knutson TR, Manabe S (1995) Time-mean response over the tropical Pacific to increased c0 2 in a coupled ocean-atmosphere model. J Clim 8:2181–2199. doi:10.1175/1520-0442(1995)008<2181:TMROTT>2.0.CO;2

Kosaka Y, Xie S-P (2013) Recent global-warming hiatus tied to equatorial Pacific surface cooling. Nature. doi:10.1038/nature12534

Latif, M, Keenlyside NS (2009) El Niño/Southern Oscillation response to global warming. Proc Natl Acad Sci 106(49): 20578–20583

L'Heureux ML, Lee S, Lyon B (2013) Recent multidecadal strengthening of the Walker circulation across the tropical Pacific. Nat Clim Change 3:1–6. doi:10.1038/nclimate1840

Luo J–J, Sasaki W, Masumoto Y (2012) Indian Ocean warming modulates Pacific climate change. Natl Acad Sci, Proc. doi:10.1073/pnas.1210239109

Meehl G, Washington W (1996) El Niño-like climate change in a model with increased atmospheric CO 2 concentrations. Nature 382:56–60

Meehl GA, Covey C, Delworth T, Latif M, McAvaney B, Mitchell JFB, Stouffer RJ, Taylor KE (2007) THE WCRP CMIP3 multimodel dataset: a new era in climate change research. Bull Am Meteorol Soc 88:1383. doi:10.1175/BAMS-88-9-1383

Meng Q, Latif M, Park W, Keenlyside NS, Semenov VA, Martin T (2011) Twentieth century Walker Circulation change: data analysis and model experiments. Clim Dyn 1–17. doi:10.1007/s00382-011-1047-8

North GR, Bell TL, Cahalan RF (1982) Sampling errors in the estimation of empirical orthogonal functions. Mon Weather Rev 110:699–706

Philander S (1990) El Niño, La Niña, and the southern oscillation. Academic, San Diego

Philip S, van Oldenborgh GJ (2009) Significant atmospheric nonlinearities in the ENSO Cycle. J Clim 22:4014–4028. doi:10.1175/2009JCLI2716.1

Power SB, Kociuba G (2010) The impact of global warming on the Southern Oscillation Index. Clim Dyn 37:1745–1754. doi:10.1007/s00382-010-0951-7

Power SB, Kociuba G (2011) What caused the observed 20th century weakening of the Walker circulation? J Clim. 1106291453 25000. doi:10.1175/2011JCLI4101.1

Power S, Casey T, Folland C, Colman A, Mehta V (1999) Inter-decadal modulation of the impact of ENSO on Australia. Clim Dyn 15:319–324

Rodgers KB, Friederichs P, Latif M (2004) Tropical Pacific decadal variability and its relation to decadal modulations of ENSO. J Clim 17:3761–3774. doi:10.1175/1520-0442(2004)017<3761:TPDVAI>2.0.CO;2

Schwendike J, Govekar P, Reeder MJ, Wardle R, Berry GJ, Jakob C (2014) Local partitioning of the overturning circulation in the tropics and the connection to the Hadley and Walker circulation. J Geophys Res Atmos. doi:10.1002/2013JD020742

Simmons A, Uppala S, Dee D, Kobayashi S (2007) ERA-Interim: new ECMWF reanalysis products from 1989 onwards. ECMWF Newsl 110:25–35

Singh MS, O'Gorman PA (2012) Upward shift of the atmospheric general circulation under global warming: theory and Simulations. J Clim 25:8259–8276. doi:10.1175/JCLI-D-11-00699.1

Sohn BJ, Park S-C (2010) Strengthened tropical circulations in past three decades inferred from water vapor transport. J Geophys Res 115:D15112. doi:10.1029/2009JD013713

Solomon A, Newman M (2012) Reconciling disparate twentieth-century Indo-Pacific ocean temperature trends in the instrumental record. Nat Clim Change 2:691–699. doi:10.1038/nclimate1591

Taylor KE, Stouffer RJ, Meehl GA (2012) An overview of CMIP5 and the experiment design. Bull Am Meteorol Soc 93:485–498. doi:10.1175/BAMS-D-11-00094.1

Tokinaga H, Xie S-P, Deser C, Kosaka Y, Okumura YM (2012a) Slowdown of the Walker circulation driven by tropical Indo-Pacific warming. Nature 491:439–443. doi:10.1038/nature11576

Tokinaga H, Xie S-P, Timmermann A, McGregor S, Ogata T, Kubota H, Okumura YM (2012b) Regional patterns of tropical Indo-Pacific climate change: evidence of the Walker circulation weakening*. J Clim 25:1689–1710. doi:10.1175/JCLI-D-11-00263.1

Vecchi GA, Soden BJ (2007) Global warming and the weakening of the tropical circulation. J Clim 20:4316–4340. doi:10.1175/JCLI4258.1

Vecchi GA, Soden BJ, Wittenberg AT, Held IM, Leetmaa A, Harrison MJ (2006) Weakening of tropical Pacific atmospheric circulation due to anthropogenic forcing. Nature 441:73–76. doi:10.1038/nature04744

Yu J-Y, Kim ST (2011) Reversed spatial asymmetries between El Niño and La Niña and their linkage to decadal ENSO modulation in CMIP3 models. J Clim. 110506133859050. doi:10.1175/JCLI-D-11-0024.1

Yu B, Zwiers FW (2010) Changes in equatorial atmospheric zonal circulations in recent decades. Geophys Res Lett 37:L05701

Yu B, Zwiers FW, Boer GJ, Ting MF (2012) Structure and variances of equatorial zonal circulation in a multimodel ensemble. Clim Dyn. doi:10.1007/s00382-012-1372-6